

## Article

# A High-Accuracy Thermal Conductivity Model for Water-Based Graphene Nanoplatelet Nanofluids

Elif Begum Elcioglu

Department of Mechanical Engineering, Eskişehir Technical University, 26555 Eskişehir, Turkey; ebelcioglu@eskisehir.edu.tr

**Abstract:** High energetic efficiency is a major requirement in industrial processes. The poor thermal conductivity of conventional working fluids stands as a limitation for high thermal efficiency in thermal applications. Nanofluids tackle this limitation by their tunable and enhanced thermal conductivities compared to their base fluid counterparts. In particular, carbon-based nanoparticles (e.g., carbon nanotubes, graphene nanoplatelets, etc.) have attracted attention since they exhibit thermal conductivities much greater than those of metal-oxide and metallic nanoparticles. In this work, thermal conductivity data from the literature are processed by employing rigorous statistical methodology. A high-accuracy regression equation is developed for the prediction of thermal conductivity of graphene nanoplatelet-water nanofluids, based on the temperature (15–60 °C), nanoparticle weight fraction (0.025–0.1 wt.%), and graphene nanoparticle specific surface area (300–750 m<sup>2</sup>/g). The strength of the impact of these variables on the graphene nanoplatelet thermal conductivity data can be sorted from the highest to lowest as temperature, nanoparticle loading, and graphene nanoplatelet specific surface area. The model developed by multiple linear regression with three independent variables has a determination coefficient of 97.1% and exhibits convenience for its ease of use from the existing prediction equations with two independent variables.



**Citation:** Elcioglu, E.B. A High-Accuracy Thermal Conductivity Model for Water-Based Graphene Nanoplatelet Nanofluids. *Energies* **2021**, *14*, 5178. <https://doi.org/10.3390/en14165178>

Academic Editor: Helena Maria Rodrigues Gonçalves

Received: 2 August 2021  
Accepted: 18 August 2021  
Published: 21 August 2021

**Publisher's Note:** MDPI stays neutral with regard to jurisdictional claims in published maps and institutional affiliations.



**Copyright:** © 2021 by the author. Licensee MDPI, Basel, Switzerland. This article is an open access article distributed under the terms and conditions of the Creative Commons Attribution (CC BY) license (<https://creativecommons.org/licenses/by/4.0/>).

**Keywords:** nanofluids; multiple regression; correlation; thermal conductivity; graphene

## 1. Introduction

After the pioneering work of Choi and Eastman [1], nanofluids as homogeneous mixtures of nanoparticles and liquids have attracted significant interest mainly due to the potential of high thermal conductivity compared to the conventional heat transfer fluids. In addition to thermal conductivity, nanofluids' thermophysical properties and heat transfer characteristics being highly tunable made them promising materials in a variety of systems, including heat pipes [2], heat exchangers [3], and solar energy systems [4] as well as in applications including microchip cooling [5], nuclear cooling [6], machining [7], and enhanced oil recovery [8]. On the other hand, it has long been one of the important points to understand and maintain the main features of a nanofluid, which include steady state suspension, colloidal stability, and unchanging chemical nature of the base fluid [9]. The enhancements reported in the thermal conductivity of nanofluids have directed the research in this area primarily in thermal properties and heat transfer. One of the remarkable enhancements in thermal conductivity of nanofluids has been reported by Xuan and Li [10]: more than 70% at nearly 8% nanoparticle volume fraction for CuO-water nanofluids.

Although spherical and nearly-spherical nanoparticles' dispersions have been investigated in detail, non-spherical nanoparticles with shape-induced characteristics exhibit new and interesting properties. In particular, carbon-based nanomaterials not only exhibit high thermal conductivity but also lightness and high surface area, and outstanding chemical, mechanical, and electrical properties [11]. Pavia et al. [11] reviewed different versions of graphene (i.e., graphene oxide, graphene nanoplatelets (GNPs), graphene nanosheet, etc.) and reported on the graphene nanoparticle nanofluids' preparation conditions and thermal conductivities. Le Ba et al. [9] reviewed the preparation and stability of graphene

nanoparticle nanofluids. They also mentioned some potential applications of graphene based nanofluids, such as sensors, micro and mini channels, composite materials, automobiles, and so on. Hilo et al. [12] reviewed graphene nanofluids preparation, stability, and thermophysical properties, along with convective heat transfer performance results from the literature.

Bahaya et al. [13] studied GNP-water nanofluids and reported 1.43 times increase in thermal conductivity over water at a nanoparticle volume fraction of 0.0014, noting more than 30 times increased viscosity at this concentration. Iranmanesh et al. [14] reported on the effects of the specific surface area, temperature, and nanoparticle concentration on the thermal conductivity and viscosity of GNP-water nanofluids. Based on their experimental work, they performed statistical analysis for quantifying these parameters impacts. Their results revealed that the sole effects of temperature, specific surface area, and concentration were significant, as well as their two-factor and more complex interactions on the thermal conductivity. They also presented two predicting equations for the thermal conductivity of GNP-water nanofluids for 500 m<sup>2</sup>/g and 750 m<sup>2</sup>/g GNP specific surface areas. Naghash et al. [15] studied nano-porous graphene-water nanofluids of 0.025–0.1 wt.% with a graphene specific surface area of 814 m<sup>2</sup>/g. They reported that the enhancement in thermal conductivity of the 0.1 wt.% nanofluid was poor (3.8%), while the enhancement in the convective heat transfer coefficient was high (34%). Mehrali et al. [16] studied GNP-water nanofluids of 0.025–0.1 wt.% concentrations with GNP specific surface areas of 300, 500, and 750 m<sup>2</sup>/g. Their measurements showed that the highest enhancement in thermal conductivity was more than 27% at the highest concentration (0.1 wt.%) and GNP specific surface area (750 m<sup>2</sup>/g). Sarsam et al. [17] examined water-based triethanolamine-treated GNP nanofluids' stability and thermophysical properties based on GNP specific surface areas (300, 500, and 750 m<sup>2</sup>/g). Their results showed that thermal conductivity of GNP-water nanofluids increased at 0.1 wt.% as the GNP specific surface area increased. Yarmand et al. [18] studied functionalized GNP-water nanofluids' thermophysical properties and heat transfer performance in a square pipe. Thermal conductivity of the 0.1 wt.% samples increased by 13.56% with respect to water at 293 K. In some studies, experimental works on graphene nanofluids were accompanied by soft-computing methods as well. Khosrojerdi [19] measured the thermal conductivity of GNP-water nanofluids with a GNP diameter < 2 μm and 750 m<sup>2</sup>/g specific surface area, and performed multilayer perceptron (MLP) artificial neural network (ANN) analysis for the prediction of the experimental data. They considered the following temperature and nanoparticle weight percentages: 25–50 °C and 0.00025–0.005. Their model had a determination coefficient of  $R^2 = 96.8\%$ , successfully representing the experimental dataset. Tahani et al. [20] measured and then modeled water-based graphene oxide nanoplatelet nanofluids' (of 0.001–0.045 weight fractions) thermal conductivity within a temperature range of 25–50 °C. They reported that their MLP-ANN based model had a determination coefficient of  $R^2 = 99\%$ .

Such tunable and outstanding properties of GNP nanoparticle nanofluids gave rise to application-based investigations, including microchannels [21], counterflow heat exchangers [22], automobile radiators [23], and cooling systems of wind turbine generators [24] to name a few. Apart from those applications, GNP nanofluid performances in solar thermal and convective heat transfer systems have been investigated. Sani et al. [25] studied 50:50% vol. of Havoline XLC and water mixture-based polycarboxylate modified GNP nanofluids (with SDBS as surfactant) for solar thermal applications, highlighting the possibility of a highly tunable solar absorption. Vallejo et al. [26] studied water-based polycarboxylate chemically modified graphene nanoplatelets (P-GnP) and sulfonic acid-functionalized graphene nanoplatelets (S-GnP) nanofluids of 0.005–0.05 wt.% for their stability and optical properties. They reported that at 0.025 wt.% concentration, the spectral extinction coefficient for P-GnP was around two times higher than that of S-GnPs from 300 nm to higher wavelengths, rendering P-GnPs a better absorber. Agromayor et al. [27] investigated the thermophysical properties and heat transfer performance of aqueous GNP nanofluids of 0.25–1 wt.%. The GNPs were functionalized with sulfonic acid to assist their dispersion in

water. Enhancements in heat transfer coefficient were observed for 0.25–0.75 wt.% nanofluids, and the optimum heat transfer coefficient was exhibited by 0.5 wt.% nanofluid as 32% compared to water. Akhavan-Zanjani et al. [28] studied the heat transfer performance of graphene nanosheet-water nanofluids and reported increases in thermal conductivity and heat transfer coefficient under laminar flow of around 10% and 14%, respectively. Ali and Arshad [29] studied a pin fin heat sink channel with GNP-water nanofluid as the working fluid. In the formulation of nanofluid, they used PVP at a weight that was equal to that of the GNPs and reported that the nanofluid was stable for two months. Mehrali et al. [30] evaluated the performance of GNP-water nanofluids for turbulent flow based on the GNP specific surface area (i.e., 300, 500, and 750 m<sup>2</sup>/g). Their results showed that the heat transfer coefficient increased with the nanoparticle loading and GNP specific surface area. Sadeghinezhad et al. [31] used GNP-water nanofluids in sintered heat pipes and investigated the effects of GNP concentration (0.025–0.1 wt.%), heat pipe inclination, and power input. Their results showed that the best performance was exhibited by the highest concentration sample (0.1 wt.%), which reduced the thermal resistance by 48.4% at a tilt angle of 60° and 80 W input power. Iranmanesh et al. [32] assessed GNP-water nanofluids (with GNP specific surface area of 750 m<sup>2</sup>/g) with 0.025–0.1 wt.% in an evacuated tube solar collector system. They reported around a 90% increase in thermal efficiency at a flow rate of 0.000025 m<sup>3</sup>/s. Keklikcioglu et al. [33] reported on GNP-water nanofluids thermal and hydrodynamic behavior as well as their thermophysical properties. They reported on a predicting equation for the thermal conductivity of GNP-water nanofluids of 3 nm particle size and 0.5–1 wt.%. Arzani et al. [34] investigated thermal performance of covalent (GNP-COOH) and non-covalent (GNP-SDBS) functionalized GNP-water nanofluids in an annular heat exchanger. They considered the following ranges for temperature, Reynolds number, and nanoparticle weight concentration: 293–353 K, 5000–17,000, and 0.025–0.1%, respectively. The GNP-SDBS samples with 0.1 wt.% and 0.05 wt.% exhibited the highest two Nusselt numbers and heat transfer coefficients, followed by 0.1 wt.% GNP-COOH.

The literature review shows that there is considerable interest in graphene-based nanofluids, especially due to the promising thermal characteristics of graphene and the promising stability enhancements obtained (for example, see the work by [18]). In this regard, the motivation of this work is to develop a high-accuracy regression equation that can be used for the prediction of GNP-water nanofluids' thermal conductivity. The model includes temperature, nanoparticle loading, and GNP specific surface area as independent variables.

## 2. Materials and Methods

### 2.1. Materials Considered in This Work

The objective of this work is to develop a predicting equation for the thermal conductivity of GNP-water nanofluids based on the GNP specific surface area, GNP concentration, and temperature. Figure 1 comparatively shows some of the metal-oxide and carbon-based nanoparticles' thermal conductivity enhancements over water. It can be observed that the thermal conductivity enhancement with graphene is more than two orders of magnitude greater than those of TiO<sub>2</sub> and Al<sub>2</sub>O<sub>3</sub> and also greater than that with carbon nanotubes (CNTs).

One other reason of the importance of the thermal conductivity of GNP nanofluids is their potential in energetic applications. Such predictions should be based on material and process parameters (with significant effects) so that the dependent variable can be quantified. Table 1 summarizes the important morphological variables of the GNP-water nanofluid works from the literature. It is observed that the concentration and specific surface area are important variables, which were observed to be controllably and carefully varied in the previous works (see for example [16,17,30] for the effect of GNP specific surface area) in order to observe their impacts on thermophysical properties and performance.

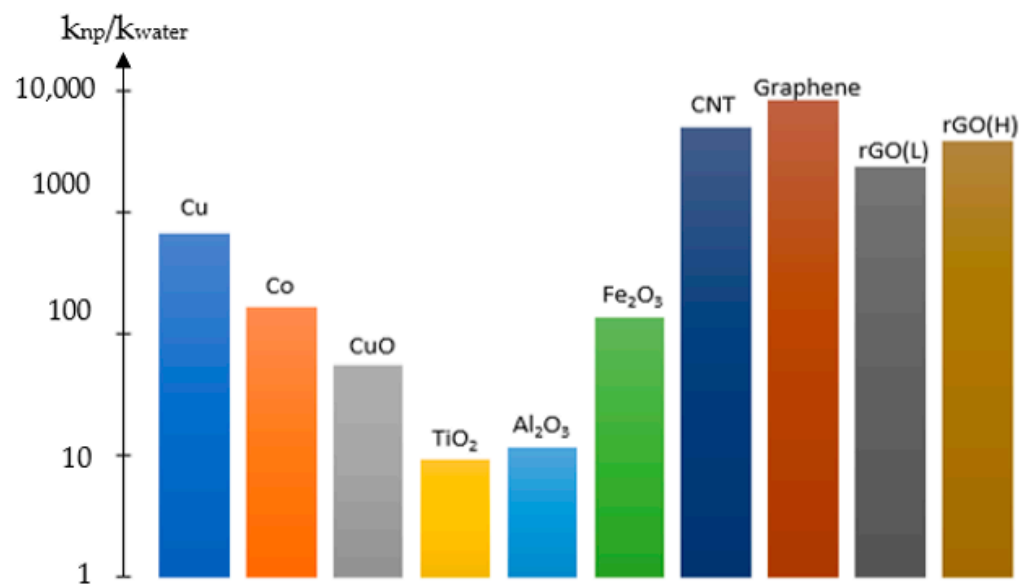


**Figure 1.** Thermal conductivity ratios (in log-scale) of the nanoparticle materials to thermal conductivity of water at 293 K. Nanoparticle and water thermal conductivity values are taken from [11]. Abbreviations: L: lower limit, H: upper limit of the thermal conductivity value.

**Table 1.** Parameter summary of the previous works on the GNP-water nanofluids.

Reference	Concentration ■ (%)	Details
Agromayor et al. [27]	0.025, 0.05, 0.075, 0.1	GNPs were sulfonic acid- functionalized.
Ali and Arshad [29]	10	GNP and PVPs added in equal concentration. $d^* = 5\text{--}10\ \mu\text{m}$
Iranmanesh et al. [32]	0.025, 0.05, 0.075, 0.1	$SSA^{**} = 750\ \text{m}^2/\text{g}$
Iranmanesh et al. [14]	0.05, 0.075, 0.1	$SSA = 500\ \text{m}^2/\text{g}, 750\ \text{m}^2/\text{g}$ $d = 2\ \mu\text{m}, t^{***} = 2\ \text{nm}$
Keklikcioglu et al. [33]	0.5, 0.75, 1	Particle size = 3 nm
Mehrli et al. [16]	0.025, 0.05, 0.075, 0.1	$SSA = 300\ \text{m}^2/\text{g}, 500\ \text{m}^2/\text{g}, 750\ \text{m}^2/\text{g}$ $d = 2\ \mu\text{m}, t = 2\ \text{nm}$
Sami Sarsam et al. [17]	0.025, 0.05, 0.075, 0.1	GNPs were triethanolamine-treated. $SSA = 300\ \text{m}^2/\text{g}, 500\ \text{m}^2/\text{g}, 750\ \text{m}^2/\text{g}$ $d = 2\ \mu\text{m}, t = 2\ \text{nm}$ $SSA \geq 600\ \text{m}^2/\text{g}$
Zhou et al. [35]	1.2–16.7 (vol.)	Sheet size: $0.1\text{--}3\ \mu\text{m}, t = 1\ \text{nm}$
Yarmand et al. [18]	0.02, 0.04, 0.06, 0.1	HNO <sub>3</sub> and H <sub>2</sub> SO <sub>4</sub> functionalized GNPs. $SSA = 500\ \text{m}^2/\text{g}, d = 2\ \mu\text{m}, t = 2\ \text{nm}$

■ In weight, unless otherwise stated. Abbreviations: \*  $d$ : diameter, \*\*  $SSA$ : specific surface area, \*\*\*  $t$ : thickness.

## 2.2. Methodology of This Work

In this work, thermal conductivity data reported by Iranmanesh et al. [14] and Mehrli et al. [16] are processed in order to quantify the impacts of the GNPs specific surface area, concentration in water, and nanofluid temperature on the aqueous GNP nanofluids thermal conductivity and to propose a new prediction equation. Overall, 96 datapoints are digitized from references ([14–16]), and multiple linear regression (MLR) analysis has been performed. Multiple regression provides information on the relationship between the dependent (response) variable ( $y$ ) and the independent (predictor) variables ( $x_i$ ), and can be used for forecasting of  $y$  based on  $x_i$ 's by means of a useful representation of the reality as the output of the regression analysis [36]. The MLR model can be written as in Equation (1):

$$y = \beta_0 + \beta_1 x_1 + \dots + \beta_i x_i + e_i \quad (1)$$

where  $\beta_0$  is the constant,  $\beta_1$  to  $\beta_i$  is the regression coefficient of each independent variable, and  $e_i$  is the error term. In order for the MLR analysis to be performed, the following assumptions should be validated [37]:

- The response variable is continuous. The predictor variables are continuous or binary;
- The response variable and predictor variables are linearly related;
- The residuals are normally distributed and homoscedastic;
- The independent variables exhibit no more than the limited multi-collinearity;
- There should not be any variable exhibiting a strong relationship with the response variable excluded from the model;
- Errors and observations are independent.

In order for the second assumption to be valid, the correlation coefficients ( $r$ ) between each independent variable and dependent variable should be  $>0.30$ . In addition, it is preferred not to have strong correlations between the independent variables. Table 2 shows the correlation coefficients between dependent and independent variables as blue marked, and the correlations being significant (Sig. (1-tailed)  $< 0.05$ ). The insignificant correlations between the independent variables are also marked as green (with significance values  $> 0.05$ ).

**Table 2.** Associations between the dependent and independent variables.

		$k_{nf}$	$\varphi$ (%)	SSA	$T$
Pearson Correlation	$k_{nf}$	1.000	0.531	0.514	0.736
	$\varphi$ (%)	<b>0.531</b>	1.000	<b>0.004</b>	<b>0.084</b>
	SSA	<b>0.514</b>	0.004	1.000	<b>0.082</b>
	$T$	<b>0.736</b>	0.084	0.082	1.000
Sig. (1-tailed)	$k_{nf}$		0.000	0.000	0.000
	$\varphi$ (%)	<b>0.000</b>		<b>0.486</b>	<b>0.208</b>
	SSA	<b>0.000</b>	0.486		0.212
	$T$	<b>0.000</b>	0.208	0.212	
$N$	$k_{nf}$	96	96	96	96
	$\varphi$ (%)	96	96	96	96
	SSA	96	96	96	96
	$T$	96	96	96	96

Another underlying assumption states that both the dependent and independent variables should exhibit multivariate normal distribution, and they should not contain outliers. This can be verified by computing the Cook's distance and Mahalanobis distance. These values are calculated and stored for each of the 96 datasets. The Cook's distance indicates the change in the regression coefficients upon removal of a value from the model [38]. If the Cook's distance value is greater than 1, then that dataset should not be included in the analysis [38]. The Mahalanobis distance is a standardized measure of an independent variable's differentiation from the dependent variable [38]. When there are three independent variables, the critical Mahalanobis distance is 16.27. The cases with Mahalanobis distance value greater than the critical Mahalanobis distance should be removed from the analyzed dataset. Table 3 shows the range of the Cook's distance and Mahalanobis distance values of the dataset considered in this work. As shown, the maximum Cook's distance value is 0.132 ( $<1$ ) and the maximum Mahalanobis distance value is 8.835 ( $<16.27$ ), both in line with the criteria.

**Table 3.** Regression diagnostics: the residual values, Mahalanobis distance, and Cook's distance.

	Min.	Max.	Mean	Std. Deviation	N
Predicted Value	0.5919	0.8529	0.7047	0.05120	96
Std. Predicted Value	−2.204	2.894	0.000	1.000	96
Std. Error of Predicted Value	0.001	0.003	0.002	0.000	96
Adjusted Predicted Value	0.5913	0.8530	0.7048	0.05122	96
Residual	−0.01776	0.02467	0.00000	0.00880	96
Std. Residual	−1.985	2.758	0.000	0.984	96
Stud. Residual	−2.032	2.811	−0.002	1.006	96
Deleted Residual	−0.01861	0.02562	−0.00003	0.00921	96
Stud. Deleted Residual	−2.068	2.924	0.000	1.017	96
<b>Mahalanobis Distance</b>	<b>0.250</b>	<b>8.835</b>	2.969	1.772	96
<b>Cook's Distance</b>	<b>0.000</b>	<b>0.132</b>	0.012	0.019	96
Centered Leverage Value	0.003	0.093	0.031	0.019	96

In order to check for the fourth assumption on multi-collinearity, the correlation coefficients between the independent variables should be  $<0.70$ . As shown, the correlation coefficients between the variables are all lower than 0.7. Multi-collinearity can also be checked by considering tolerance, variance inflation factor (VIF), and condition indices (CI). As a rule of thumb, tolerance  $> 0.1$ , VIF  $< 10$  [37] (to avoid multi-collinearity problems), and CI  $< 30$  are required. As shown in Table 4, these conditions are satisfied; hence, there is no multi-collinearity problem.

**Table 4.** Collinearity statistics and condition index values.

Model		Collinearity Statistics				
		Tolerance		VIF		
1	Constant					
	$\varphi$ (%)		0.993		1.007	
	SSA		0.993		1.007	
	T		0.986		1.014	
Dimension	Eigenvalue	Condition Index	Variance Proportions			
			Constant	$\varphi$ (%)	SSA	T
1	3.728	<b>1.000</b>	0.00	0.01	0.01	0.01
2	0.131	<b>5.333</b>	0.00	0.77	0.08	0.19
3	0.106	<b>5.941</b>	0.01	0.01	0.43	0.62
4	0.035	<b>10.294</b>	0.99	0.21	0.49	0.18

Finally, the distribution of the residuals being normal or not can be controlled by checking the scatter plot obtained for the residuals. Figure 2a shows that the residuals are normally distributed since the data markers are located very near the diagonal. Figure 2b also reveals that the residuals distribution is normal and homoscedastic, as the data markers are randomly distributed without showing any pattern [32].

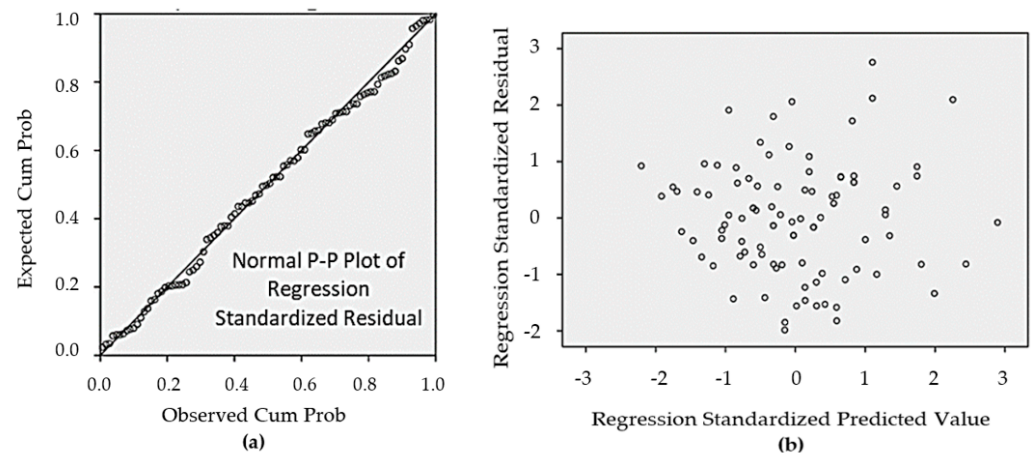


**Figure 2.** Normal distribution and homoscedastic behavior of the residuals via (a) a normal P-P plot of regression and (b) a scatter plot.

### 3. Results

In this work, the question of whether the thermal conductivity of GNP nanofluids is being influenced by the GNP's specific surface area, temperature, and GNP's concentration is evaluated using MLR analysis. The developed MLR model is found to be valid, as shown in Table 5 below (Sig. < 0.05).

**Table 5.** Test of the validity of the MLR model.

ANOVA						
Model		Sum of Squares	df	Mean Square	F	Sig.
1	Regression	0.249	3	0.083	1037.122	0.000
	Residual	0.007	92	0.000		
	Total	0.256	95			

The predictive power of specific surface area, concentration, and temperature is shown in Table 6. According to the results shown, it is observed that the GNPs' specific surface area, GNP's concentration, and temperature taken together explains 97.1% of the GNPs' thermal conductivity. The  $R^2$  value being very close to 1 indicates good predictive power of the used independent variables ( $\varphi$  (%), SSA, and  $T$ ) of the dependent variable [36].

**Table 6.** Results showing independent variables explanation of the dependent variable.

Model Summary			
Model	R	$R^2$	Adjusted $R^2$
1	0.986	0.971	0.97

Having confirmed the validity of the MLR model, the prediction equation is developed. Table 7 shows the coefficients of the predictor variables.

**Table 7.** Model parameter values.

	Unstandardized Coefficients		Standardized Coefficients		t	Sig.
	B	Std. Error	Beta			
Constant	0.485	0.004			116.767	0.000
$\varphi$ (%)	0.925	0.035	0.474		26.734	0.000
SSA	0.000	0.000	0.458		25.819	0.000
$T$	0.003	0.000	0.658		37.002	0.000

Table 7 shows that all the predictor variables are statistically significant (for all, Sig. < 0.05). Although the unstandardized coefficient of *SSA* appears to be 0, its presence is statistically significant as its significance value is <0.05, and it should be included in the model. The main reason for this is the range of the *SSA* variable values (300–750) being considerably greater than the range of the other two variables. In this case, it is convenient to include *SSA* as a parameter in the prediction model with a coefficient of 0.0001. From the outputs of Table 7, the prediction equation can be written as in Equation (2).

$$k_{nf} = 0.485 + 0.925\varphi + 0.0001 \text{ SSA} + 0.003T \quad (2)$$

In Equation (2),  $\varphi$  is in wt. (%),  $T$  is in °C, and *SSA* is in m<sup>2</sup>/g. The ranges of the independent variables are (0.025–0.1 wt.%), 15–60 °C, and 300–750 m<sup>2</sup>/g, respectively, for  $\varphi$ ,  $T$ , and *SSA*. One other conclusion from Table 7 is about comparison of the strengths of  $\varphi$ , *SSA*, and  $T$  on  $K_{nf}$ , based on the beta values. The parameter with the highest absolute beta value is the parameter with the strongest effect. In this regard, the effects of the parameters can be sorted from highest to lowest as  $T$ ,  $\varphi$ , and *SSA*.

#### 4. Discussion

Figure 3a–c shows the comparison of the predictions of the developed regression equation (i.e., Equation (2)) against the experimental data reported by [14,16]. The legends of Figure 3a–c are abbreviated for convenience so that Dataset-1 is the data by Mehrali et al. [16], and Dataset-2 is the data by Iranmanesh et al. [14]. Good coverage and inclusion of the model on both the datasets can be observed. The comparisons are limited to these datasets, since other GNP thermal conductivity works were concerned with functionalized GNP nanofluids (e.g., [17,18]) and/or GNPs of different morphologies (e.g., [15,33]).

The developed model and its mathematical form can also be compared against the existing models. Iranmanesh et al. [14], after an elaborated statistical methodology, proposed correlating equations for GNP-water nanofluid thermal conductivity individually for *SSA*'s of 500 m<sup>2</sup>/g and 750 m<sup>2</sup>/g in the form of  $k_{nf}(SSA) = f(T, \varphi)$ . Keklikcioglu et al. [33] also proposed correlating equations for the GNP-water nanofluid thermal conductivity individually for the nanoparticle concentrations of 0.5, 0.75, and 1 wt.% in the form of  $k_{nf}(\varphi) = f(T)$ . To the best of the author's knowledge, the mentioned models were the only ones so far proposed in the prediction of the thermal conductivity of GNP-water nanofluids. The regression model developed in this current work, i.e., Equation (2) with the following form  $k_{nf} = f(T, \varphi, SSA)$ , enables prediction of the thermal conductivity based on  $T$ ,  $\varphi$ , and *SSA* via the usage of a single equation, which is expected to exhibit a higher ease of utility.

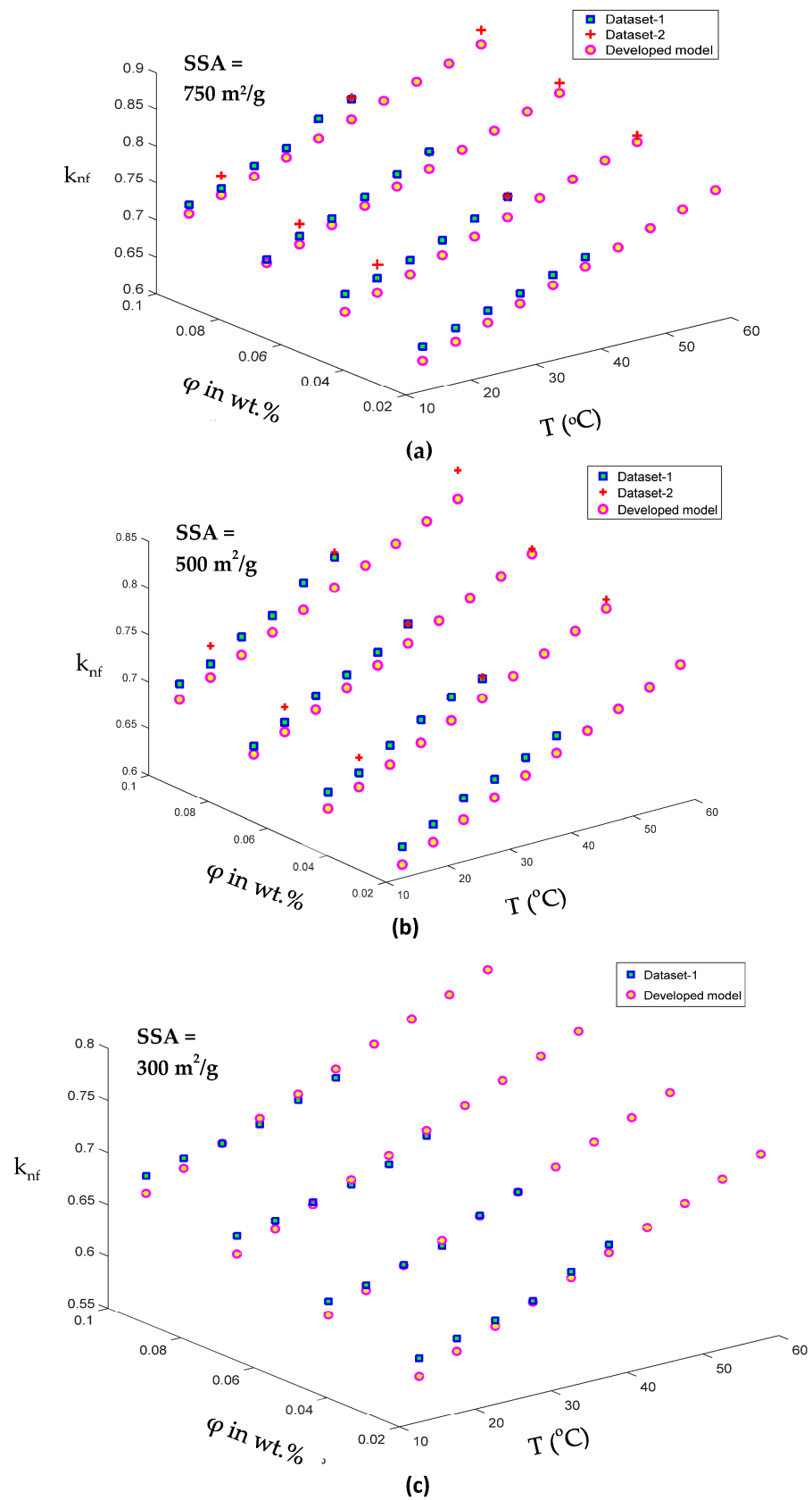


**Figure 3.** Comparison of the predictions of Equation (2) against the experimental data by [14] and [16] for GNP specific surface areas of (a) 750 m<sup>2</sup>/g, (b) 500 m<sup>2</sup>/g, and (c) 300 m<sup>2</sup>/g.

## 5. Conclusions

In this work, a new and high-predictive power equation for the estimation of thermal conductivity of GNP-water nanofluids has been developed by using rigorous statistical analysis based on the multiple linear regression method. The model has been developed based on the data reported by [14,16] for GNPs of 2  $\mu\text{m}$  diameter and 2 nm thickness. The independent variable intervals for which the model is developed are 15–60  $^{\circ}\text{C}$ , 300–750  $\text{m}^2/\text{g}$ , and 0.025–0.1 wt.%. The developed model has a very high  $R^2$  value of 97.1% and includes the nanoparticle loading, temperature, and the GNPs' specific surface area as independent variables. The inclusion of these three variables is important for the convenience and ease of the usage of the regression model (as a single prediction tool).

**Funding:** This research received no external funding.

**Data Availability Statement:** Not applicable.

**Conflicts of Interest:** The author declares no conflict of interest.

## References

1. Choi, S.U.S.; Eastman, J.A. Enhancing Thermal Conductivity of Fluids with Nanoparticles. In Proceedings of the 1995 International Mechanical Engineering Congress and Exhibition, San Francisco, CA, USA, 12–17 November 1995.
2. Nazari, M.A.; Ahmadi, M.H.; Sadeghzadeh, M.; Shafii, M.B.; Goodarzi, M. A review on application of nanofluid in various types of heat pipes. *J. Cent. South Univ.* **2019**, *26*, 1021–1041. [[CrossRef](#)]
3. Shirzad, M.; Ajarostaghi, S.S.M.; Delavar, M.A.; Sedighi, K. Improve the thermal performance of the pillow plate heat exchanger by using nanofluid: Numerical simulation. *Adv. Powder Technol.* **2019**, *30*, 1356–1365. [[CrossRef](#)]
4. Verma, S.K.; Tiwari, A.K. Progress of nanofluid application in solar collectors: A review. *Energy Convers. Manag.* **2015**, *100*, 324–346. [[CrossRef](#)]
5. Ganvir, R.B.; Walke, P.V.; Kriplani, V.M. Heat transfer characteristics in nanofluid—A review. *Renew. Sustain. Energy Rev.* **2017**, *75*, 451–460. [[CrossRef](#)]
6. Sukarno, D.H. Challenges for nanofluid applications in heat transfer technology. *J. Phys. Conf. Ser.* **2017**, *795*, 012020. [[CrossRef](#)]
7. Sharma, A.K.; Tiwari, A.K.; Dixit, A.R. Progress of Nanofluid Application in Machining: A Review. *Mater. Manuf. Process.* **2015**, *30*, 813–828. [[CrossRef](#)]
8. Suleimanov, B.A.; Ismailov, F.S.; Veliyev, E.F. Nanofluid for enhanced oil recovery. *J. Pet. Sci. Eng.* **2011**, *78*, 431–437. [[CrossRef](#)]
9. Le Ba, T.; Mahian, O.; Wongwises, S.; Szilágyi, I.M. Review on the recent progress in the preparation and stability of graphene-based nanofluids. *J. Therm. Anal. Calorim.* **2020**, *142*, 1145–1172. [[CrossRef](#)]
10. Xuan, Y.; Li, Q. Heat transfer enhancement of nanofluids. *Int. J. Heat Fluid Flow* **2000**, *21*, 58–64. [[CrossRef](#)]
11. Pavía, M.; Alajami, K.; Estellé, P.; Desforges, A.; Vigolo, B. A critical review on thermal conductivity enhancement of graphene-based nanofluids. *Adv. Colloid Interface Sci.* **2021**, *294*, 102452. [[CrossRef](#)]
12. Hilo, A.; Talib, A.R.A.; Nfawa, S.R.; Sultan, M.T.H.; Hamid, M.F.A.; Bheekhun, M.I.N. Heat Transfer and Thermal Conductivity Enhancement using Graphene Nanofluid: A Review. *J. Adv. Res. Fluid Mech. Therm. Sci.* **2019**, *55*, 74–87.
13. Bahaya, B.; Johnson, D.W.; Yavuzturk, C.C. On the Effect of Graphene Nanoplatelets on Water-Graphene Nanofluid Thermal Conductivity, Viscosity, and Heat Transfer under Laminar External Flow Conditions. *J. Heat Transf.* **2018**, *140*, 064501. [[CrossRef](#)]
14. Iranmanesh, S.; Mehrali, M.; Sadeghinezhad, E.; Ang, B.C.; Ong, H.C.; Esmaeilzadeh, A. Evaluation of viscosity and thermal conductivity of graphene nanoplatelets nanofluids through a combined experimental–statistical approach using respond surface methodology method. *Int. Commun. Heat Mass Transf.* **2016**, *79*, 74–80. [[CrossRef](#)]
15. Naghash, A.; Sattari, S.; Rashidi, A. Experimental assessment of convective heat transfer coefficient enhancement of nanofluids prepared from high surface area nanoporous graphene. *Int. Commun. Heat Mass Transf.* **2016**, *78*, 127–134. [[CrossRef](#)]
16. Mehrali, M.; Sadeghinezhad, E.; Latibari, S.T.; Kazi, S.N.; Mehrali, M.; Zubir, M.N.B.M.; Metselaar, H.S.C. Investigation of thermal conductivity and rheological properties of nanofluids containing graphene nanoplatelets. *Nanoscale Res. Lett.* **2014**, *9*, 1–12. [[CrossRef](#)] [[PubMed](#)]
17. Sarsam, W.S.; Amiri, A.; Zubir, M.N.M.; Yarmand, H.; Kazi, S.N.; Badarudin, A. Stability and thermophysical properties of water-based nanofluids containing triethanolamine-treated graphene nanoplatelets with different specific surface areas. *Colloids Surfaces A Physicochem. Eng. Asp.* **2016**, *500*, 17–31. [[CrossRef](#)]
18. Yarmand, H.; Gharehkhani, S.; Shirazi, S.F.S.; Amiri, A.; Alehashem, M.S.; Dahari, M.; Kazi, S.N. Experimental investigation of thermo-physical properties, convective heat transfer and pressure drop of functionalized graphene nanoplatelets aqueous nanofluid in a square heated pipe. *Energy Convers. Manag.* **2016**, *114*, 38–49. [[CrossRef](#)]
19. Khosrojerdi, S.; Vakili, M.; Yahyaei, M.; Kalhor, K. Thermal conductivity modeling of graphene nanoplatelets/deionized water nanofluid by MLP neural network and theoretical modeling using experimental results. *Int. Commun. Heat Mass Transf.* **2016**, *74*, 11–17. [[CrossRef](#)]

20. Tahani, M.; Vakili, M.; Khosrojerdi, S. Experimental evaluation and ANN modeling of thermal conductivity of graphene oxide nanoplatelets/deionized water nanofluid. *Int. Commun. Heat Mass Transf.* **2016**, *76*, 358–365. [[CrossRef](#)]
21. Sarafraz, M.M.; Yang, B.; Pourmehran, O.; Arjomandi, M.; Ghomashchi, R. Fluid and heat transfer characteristics of aqueous graphene nanoplatelet (GNP) nanofluid in a microchannel. *Int. Commun. Heat Mass Transf.* **2019**, *107*, 24–33. [[CrossRef](#)]
22. Selvam, C.; Balaji, T.; Lal, D.M.; Harish, S. Convective heat transfer coefficient and pressure drop of water-ethylene glycol mixture with graphene nanoplatelets. *Exp. Therm. Fluid Sci.* **2017**, *80*, 67–76. [[CrossRef](#)]
23. Selvam, C.; Solaimalai, R.R.; Lal, D.M.; Harish, S. Overall heat transfer coefficient improvement of an automobile radiator with graphene based suspensions. *Int. J. Heat Mass Transf.* **2017**, *115*, 580–588. [[CrossRef](#)]
24. Vallejo, J.P.; Álvarez-Regueiro, E.; Cabaleiro, D.; Fernández-Seara, J.; Fernández, J.; Lugo, L. Functionalized graphene nano-platelet nanofluids based on a commercial industrial antifreeze for the thermal performance enhancement of wind turbines. *Appl. Therm. Eng.* **2019**, *152*, 113–125. [[CrossRef](#)]
25. Sani, E.; Vallejo, J.P.; Cabaleiro, D.; Lugo, L. Functionalized graphene nanoplatelet-nanofluids for solar thermal collectors. *Sol. Energy Mater. Sol. Cells* **2018**, *185*, 205–209. [[CrossRef](#)]
26. Vallejo, J.P.; Mercatelli, L.; Martina, M.R.; Di Rosa, D.; Dell’Oro, A.; Lugo, L.; Sani, E. Comparative study of different functionalized graphene-nanoplatelet aqueous nanofluids for solar energy applications. *Renew. Energy* **2019**, *141*, 791–801. [[CrossRef](#)]
27. Agromayor, R.; Cabaleiro, D.; Pardinás, A.A.; Vallejo, J.P.; Fernández-Seara, J.; Lugo, L. Heat transfer performance of functionalized graphene nanoplatelet aqueous nanofluids. *Materials* **2016**, *9*, 455. [[CrossRef](#)]
28. Akhavan-Zanjani, H.; Saffar-Avval, M.; Mansourkiaei, M.; Sharif, F.; Ahadi, M. Experimental investigation of laminar forced convective heat transfer of Graphene-water nanofluid inside a circular tube. *Int. J. Therm. Sci.* **2016**, *100*, 316–323. [[CrossRef](#)]
29. Ali, H.M.; Arshad, W. Effect of channel angle of pin-fin heat sink on heat transfer performance using water based graphene nanoplatelets nanofluids. *Int. J. Heat Mass Transf.* **2017**, *106*, 465–472. [[CrossRef](#)]
30. Mehrali, M.; Sadeghinezhad, E.; Rosen, M.A.; Latibari, S.T.; Mehrali, M.; Metselaar, H.S.C.; Kazi, S.N. Effect of specific surface area on convective heat transfer of graphene nanoplatelet aqueous nanofluids. *Exp. Therm. Fluid Sci.* **2015**, *68*, 100–108. [[CrossRef](#)]
31. Sadeghinezhad, E.; Mehrali, M.; Rosen, M.A.; Akhiani, A.R.; Latibari, S.T.; Mehrali, M.; Metselaar, H.S.C. Experimental investigation of the effect of graphene nanofluids on heat pipe thermal performance. *Appl. Therm. Eng.* **2016**, *100*, 775–787. [[CrossRef](#)]
32. Iranmanesh, S.; Ong, H.C.; Ang, B.C.; Sadeghinezhad, E.; Esmaeilzadeh, A.; Mehrali, M. Thermal performance enhancement of an evacuated tube solar collector using graphene nanoplatelets nanofluid. *J. Clean. Prod.* **2017**, *162*, 121–129. [[CrossRef](#)]
33. Keklikcioglu, O.; Dagdevir, T.; Ozceyhan, V. Heat transfer and pressure drop investigation of graphene nanoplatelet-water and titanium dioxide-water nanofluids in a horizontal tube. *Appl. Therm. Eng.* **2019**, *162*, 114256. [[CrossRef](#)]
34. Arzani, H.K.; Amiri, A.; Kazi, S.N.; Chew, B.T.; Badarudin, A. Experimental and numerical investigation of thermophysical properties, heat transfer and pressure drop of covalent and noncovalent functionalized graphene nanoplatelet-based water nanofluids in an annular heat exchanger. *Int. Commun. Heat Mass Transf.* **2015**, *68*, 267–275. [[CrossRef](#)]
35. Zhou, Y.; Cui, X.; Weng, J.; Shi, S.; Han, H.; Chen, C. Experimental investigation of the heat transfer performance of an oscillating heat pipe with graphene nanofluids. *Powder Technol.* **2018**, *332*, 371–380. [[CrossRef](#)]
36. Chatterjee, S.; Simonoff, J.S. *Handbook of Regression Analysis*; John Wiley & Sons, Inc.: Hoboken, NJ, USA, 2013.
37. Tranmer, M.; Murphy, J.; Elliot, M.; Pampaka, M. Multiple Linear Regression. *Cathie Marsh Inst. Work. Pap.* **2008**, *5*, 1–59.
38. Everitt, B.S.; Skrondal, A. *The Cambridge Dictionary of Statistics*; Cambridge University Press: Cambridge, UK, 2010.